

Chapter 6

Theoretical Calculations

Measurements are not validated by theory.
It's the other way round!

The differential inclusive multijet event cross-sections measured as a function of $H_{T,2}/2$, described in the previous chapter, are ~~validated by doing the comparison~~ compared with the perturbative QCD (pQCD) theoretical calculations. The lowest order (LO) calculations roughly describe the measured cross-section distributions ~~due to the dependence on the unphysical renormalization (μ_r) and factorization (μ_f) scales~~. The next-to-leading order (NLO) calculations improve the precision by reducing the dependence on μ_r and μ_f scales. This makes the NLO calculations an essential feature in the determination of fundamental parameters such as α_S and the parton distribution functions (PDFs). This chapter describes the NLO pQCD calculations used for comparison with the cross-section measurements in terms of $H_{T,2}/2$. The NLO pQCD calculations need to be corrected for the multi-parton interactions (MPI) and hadronization effects by applying non-perturbative (NP) corrections and also for the electroweak interactions (EW).

6.1 Fixed Order NLO Calculations

The NLO predictions for the differential inclusive jet event cross-sections in pQCD are computed with the NLOJET++ program version 4.1.3 [67, 68]. As explained

in Sec. 3.3.3, the interfacing of NLOJET++ program with FASTNLO [69, 70] framework is preferred over the direct calculation with NLOJET++ because with FASTNLO the calculations of the cross-sections can be repeated ~~several times with for~~ different PDFs and scale choices required for calculating the PDF and scale uncertainties. Here, FASTNLO version 2.3 framework has been used. The PDFs are accessed through the LHAPDF6 library [71, 72]. The factorization and renormalization scales are chosen equal to $H_{T,2}/2$, i.e. $\mu_f = \mu_r = H_{T,2}/2$.

In the current study, different PDF sets available for a series of different assumptions on the strong coupling constant, at the scale of the Z boson mass $\alpha_s(M_Z)$ are used for NLO calculations. Table 6.1 summarizes the existing PDF sets in LHC Run 1 (upper rows) and the newer PDF sets for Run 2 (lower rows). The different columns list the number of flavours N_f , the assumed masses M_t and M_Z of the top quark and the Z boson, respectively, the default values of $\alpha_s(M_Z)$, and the range in $\alpha_s(M_Z)$ variation available for fits with different PDF sets. All sets use a variable-flavour number scheme with at most five or six flavours apart from the ABM11 PDF, which employs a fixed-flavour number scheme with $N_F = 5$. Out of these eight PDF sets the following three are not considered further because of the below mentioned reasons :

- At NLO, predictions based on ABM11 do not describe LHC jet data at small jet rapidity [111–114].
- The HERAPDF2.0 set exclusively fits HERA DIS data with only weak constraints on the gluon PDF.
- The range of values available for $\alpha_s(M_Z)$ is too limited for the NNPDF3.0 set.

Mainly CT10 PDF set is considered for comparison between data and theory predictions as well as for calculating theoretical uncertainties.

Table 6.1: NLO PDF sets are available via LHAPDF6 with various assumptions on the value of $\alpha_s(M_Z)$. The upper rows list the existing sets in LHC Run 1 and newer ones for Run 2 are listed in lower rows, along with the corresponding number of flavours N_f , the assumed masses M_t and M_Z of the top quark and the Z boson, respectively, the default values of $\alpha_s(M_Z)$, and the range in $\alpha_s(M_Z)$ variation available for fits.

Base set	N_F	M_t (GeV)	M_Z (GeV)	$\alpha_s(M_Z)$	$\alpha_s(M_Z)$ range
ABM11 [30]	5	180	91.174	0.1180	0.110 - 0.130
CT10 [115]	≤ 5	172	91.188	0.1180	0.112 - 0.127
MSTW2008 [116, 117]	≤ 5	10^{10}	91.1876	0.1202	0.110 - 0.130
NNPDF2.3 [118]	≤ 6	175	91.1876	0.1180	0.114–0.124
CT14 [27]	≤ 5	172	91.1876	0.1180	0.111–0.123
HERAPDF2.0 [31]	≤ 5	173	91.1876	0.1180	0.110–0.130
MMHT2014 [28]	≤ 5	10^{10}	91.1876	0.1200	0.108–0.128
NNPDF3.0 [29]	≤ 5	173	91.2	0.1180	0.115–0.121

6.1.1 NLO Correction Factors

The differences between LO predictions and NLO predictions give the effect of the higher-order contributions to the pQCD predictions. These are described by an NLO correction factor, k-factor, which is derived as the ratio of cross-sections as :

$$\text{k-factor} = \frac{\sigma_{\text{NLO}}}{\sigma_{\text{LO}}} \quad (6.1)$$

The impact of the higher-order corrections is determined by the size of k-factor. The small size of k-factor indicates that the cross-section predictions are precisely described at the LO whereas the larger size hints the contributions from NLO. Figure 6.1 shows the k-factors of the NLOJET++ calculations, for inclusive 2-jet and 3-jet event cross-sections and their ratio R_{32} , using five different PDF sets. k-factor for R_{32} is obtained by taking the ratio of k-factors for inclusive 3-jet event cross-sections to that of inclusive 2-jet. The k-factors are similar for all the PDF sets in the lower region, but the differences increase in regions with larger $H_{T,2}/2$. It is observed that for inclusive 3-jet event cross-sections, k-factor jumps at the lowest $H_{T,2}/2$. This is because some jet configurations are kinematically forbidden near

the p_T cut bin i.e. 150 GeV. Since the first few bins in $H_{T,2}/2$ (below 225 GeV) still suffer from these kinematical ~~constraints~~ effects, the minimum value of $H_{T,2}/2$ studied is ~~from~~ 300 GeV.

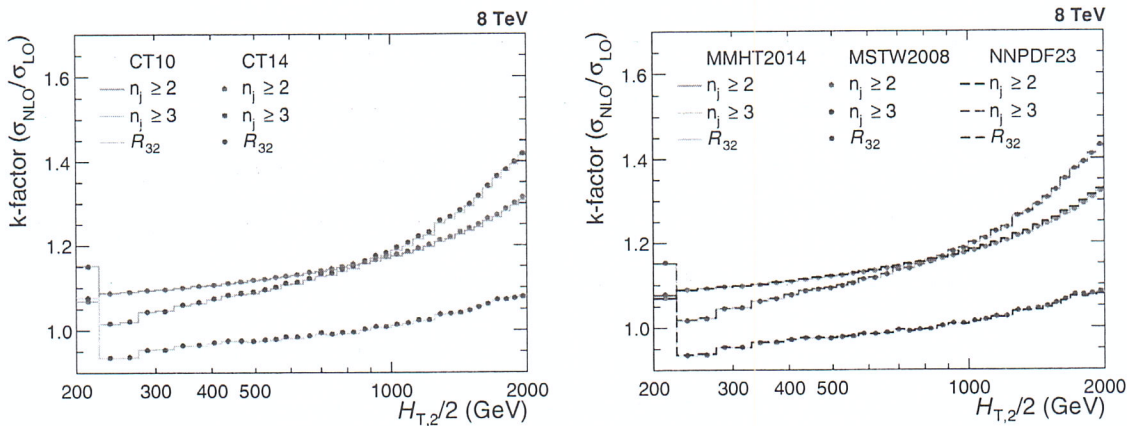


Figure 6.1: The k-factors of the NLOJET++ calculations, for inclusive 2-jet and 3-jet event cross-sections and their ratio R_{32} , using five different PDF sets.

6.1.2 Non-perturbative Corrections

The fixed-order pQCD NLO calculations predict the parton-level cross-section but lacks~~s~~ accuracy due to several effects. The partons which are emitted close to each other in phase space are not handled well in the lower order perturbation theories and hence require a parton shower (PS) correction. The scattering phenomena between partons within a colliding proton, other than the hard scattering, give rise to multi-parton interactions (MPI). The partons of the hard scattering form colorless bound states called hadrons through a process of hadronization (HAD). The MPI and hadronization cannot be modelled well within the perturbative framework. Since the fixed-order NLO calculations do not include these additional soft QCD effects, these calculations cannot be compared directly to the unfolded data. So the corrections for non-perturbative effects (NP) should be taken into account in NLO calculations. The ratio of cross-sections predicted with a nominal event generation, interfaced to the simulation of UE contributions and to the one without hadronization and MPI

effects, gives the NP correction factors which are defined as :

$$C^{\text{NP}} = \frac{\sigma^{\text{PS+HAD+MPI}}}{\sigma^{\text{PS}}} \quad (6.2)$$

In the current study, the NP effects are estimated by using samples obtained from various MC event generators with a simulation of parton shower and underlying-event (UE) contributions. The leading order (LO), HERWIG++ with the default tune of version 2.3 and PYTHIA6 with tune Z2*, and the NLO POWHEG MC event generators are considered. The matrix-element calculation is performed with POWHEG interfaced to PYTHIA8 with tune CUETS1 for the UE simulation. The ratio, defined in Eq. 6.2, is obtained for each MC generator and is fitted by a power-law function defined in Eq. 6.3. Since this ratio obtained from different MC generators have large differences, so the average of the envelope, which covers all the differences, is taken as the correction factor which is then applied as bin-by-bin multiplicative factor to the parton-level NLO cross-section. ~~The~~ ^H half of the envelope is taken as the uncertainty on the NP correction factor.

$$f(H_{\text{T},2}/2) = a \cdot (H_{\text{T},2}/2)^b + c \quad (6.3)$$

The NP correction factors, $C_{3\text{-jet}}^{\text{NP}}$ and $C_{2\text{-jet}}^{\text{NP}}$ are calculated for $n_j \geq 3$ and $n_j \geq 2$ event cross-sections, respectively and then their ratio gives the correction factor for R_{32} . The correction factors are shown in Fig. 6.2 for the inclusive 2-jet (top left) and 3-jet (top right) event cross-sections, and for the cross-section ratio R_{32} (bottom). At $H_{\text{T},2}/2 \sim 300$ GeV, the NP corrections amount to $\sim 4\text{-}5\%$ for inclusive 2-jet and 3-jet event cross-sections and $\sim 1\%$ for R_{32} , and decrease rapidly for increasing $H_{\text{T},2}/2$. On comparing the NP correction factors of R_{32} with that for individual cross-sections, it has been observed that the non-perturbative effects get reduced in R_{32} .

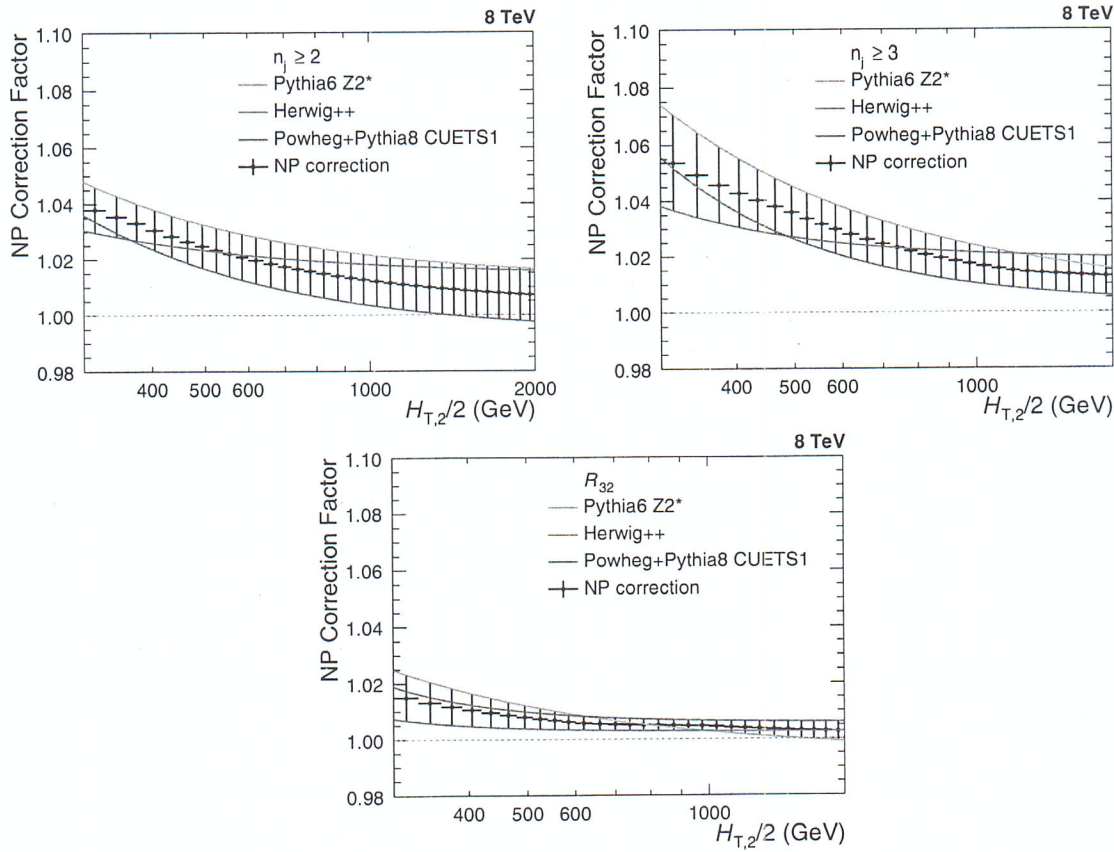


Figure 6.2: The nonperturbative (NP) corrections are presented as a function of $H_{T,2}/2$ for inclusive 2-jet (top left) and 3-jet (top right) event cross-sections, as well as their ratio R_{32} . These corrections are calculated from the leading order HERWIG++ with the default tune of version 2.3 (red line) and PYTHIA6 with tune Z2* (blue line); and the next-to-leading order POWHEG interfaced to PYTHIA8 with tune CUETS1 (green line) Monte Carlo event generators. The black solid circles give the average NP correction factor along with the uncertainty shown by the error bars.

6.1.3 Electroweak Corrections

At LHC, the center-of-mass energy of proton-proton collisions is well beyond the electroweak (EW) scale $\sim \mathcal{O}(100 \text{ GeV})$. At such a high energy, the impact of higher order EW corrections is ~~not any more negligible~~ much more with respect to QCD effects [119] and affect the jet cross-sections at large $H_{T,2}/2$. The quark-quark scattering processes involving virtual exchanges of massive W and Z bosons contribute to electroweak (EW) corrections. The fixed-order QCD calculations do not include EW corrections and hence the NLO theory calculations are corrected for EW effects. The EW correc-

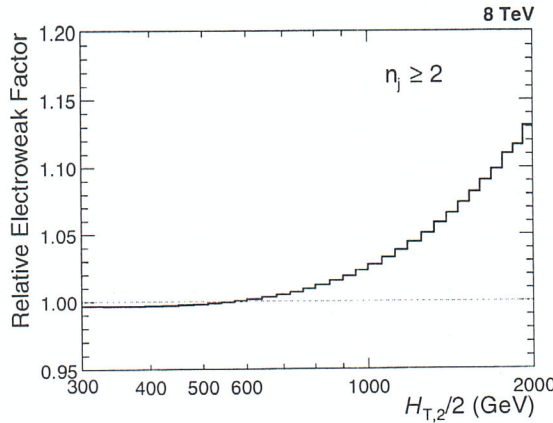


Figure 6.3: The electroweak (EW) corrections [120] in the phase space of the measurement are shown as a function of $H_{T,2}/2$ for inclusive 2-jet event cross-sections. These corrections are applied as a bin-by-bin correction factor to the fixed-order calculation of NLOJET++ as well as the MC predictions of MADGRAPH5+PYTHIA6. The EW correction factor increases up to 13% at high end of $H_{T,2}/2$ and significantly improves the agreement between data and prediction.

tions have been calculated for inclusive 1-jet and 2-jet case, in Ref. [120]. The EW correction factors in the phase space of the measurement are shown as a function of $H_{T,2}/2$ in Fig. 6.3 for inclusive 2-jet event cross-sections. These correction factor increases up to 13% at high end of $H_{T,2}/2$ which are applied as bin-by-bin correction factors to the fixed-order NLOJET++ calculations. To see the effects of EW corrections, a ratio of the data to theory predictions obtained using CT10-NLO PDF set and corrected with NP effects without including EW corrections (left) and including EW corrections (right) is plotted for inclusive 2-jet event cross-sections in Fig. 6.4. On comparing both ~~the~~ figures, it is observed that the EW corrections significantly improve the agreement between data and prediction in the high $H_{T,2}/2$ region. EW corrections are not available yet for inclusive 3-jet production and hence not applied for inclusive 3-jet event cross-sections. The guess from theory side is that EW for inclusive 2-jet and 3-jet will be similar, so for R_{32} , it is assumed to be equal to a factor of 1. Since the EW effects are not taken care of in MC simulations, these corrections are also applied to the MC predictions.

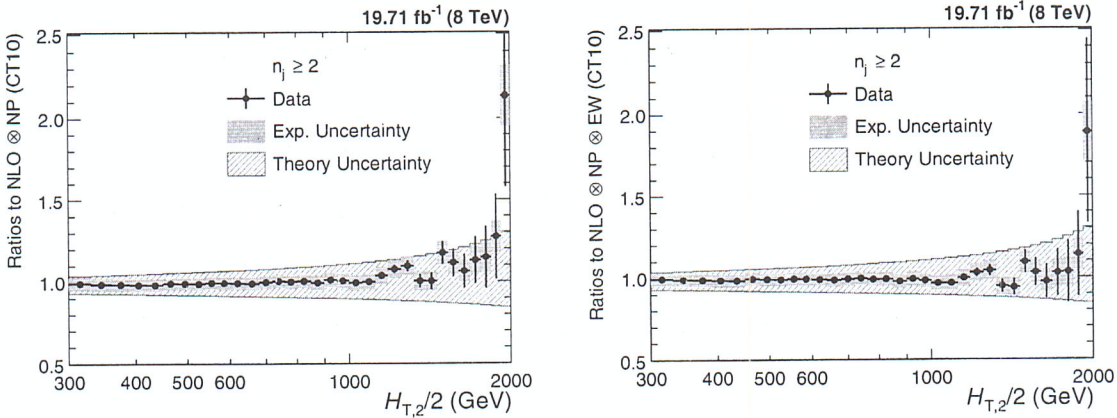


Figure 6.4: Ratio of the data over theory obtained using the CT10-NLO PDF set and corrected with non-perturbative effects (NP) without including electroweak (EW) corrections (left) and including EW corrections (right) is shown for inclusive 2-jet event cross-sections. The error bars represents the statistical uncertainty of the data and the shaded rectangles represents the total experimental systematic uncertainty. The shaded band around unity indicate the total uncertainty of the theory. The EW corrections significantly improve the agreement between data and prediction in the high $H_{T,2}/2$ region.

6.2 Theoretical Uncertainties

The measured differential inclusive multijet event cross-sections are not only sensitive to experimental uncertainties but also to the theoretical uncertainties. The renormalization and factorization scale variations, PDF uncertainties and the non-perturbative corrections contribute to theoretical uncertainties. These are described below :

6.2.1 Scale Uncertainty

In perturbative QCD calculations of cross-sections, one has to choose a renormalization (μ_r) and factorization (μ_f) scale. The dependence on scales is negligible if these calculations are performed for all orders of the perturbative series, given by Eq. 2.8. Since the NLO describes this series up to second power in α_S , it introduces a scale dependence of the measurement which is covered by systematic uncertainty known as scale uncertainty. The scale uncertainty is evaluated with the conventional recipe of varying the default scale $H_{T,2}/2$ chosen for μ_r and μ_f independently in the

following six combinations: $(\mu_r/H_{T,2}/2, \mu_f/H_{T,2}/2) = (1/2,1/2), (1/2,1), (1,1/2), (1,2), (2,1)$ and $(2,2)$. The maximal upwards and downwards deviations in cross-section from the central prediction, give the scale uncertainty. To calculate the scale uncertainty for cross-section ratio R_{32} , firstly R_{32} is obtained for each of the above mentioned scale choices and then its difference from central R_{32} is taken. The scale uncertainty calculated using CT10-NLO PDF set ranges from 5% to 13% and 11% to 17% for inclusive 2-jet and 3-jet events cross-sections respectively, and from 6% to 8% for R_{32} .

6.2.2 PDF Uncertainty

The calculation of jet cross-sections in proton-proton collisions relies upon the knowledge of PDFs. These PDF sets are obtained by global fits to all the available deep inelastic scattering (DIS) and related hard scattering data from different experiments. The various sources affect the PDFs such as the theory model, input parameters like the strong coupling constant α_S , the quark masses and the statistical and systematic uncertainty sources of the data included in the PDF fit. These sources contribute to PDF uncertainty which is evaluated according to the prescriptions given for each PDF set. The CT10-NLO PDF set [115, 121] employs the eigenvector method to evaluate the PDF uncertainties. The CT10-PDF set consists of $N_{\text{ev}} = 26$ eigenvectors with two PDF members per eigenvector k , which are varied upwards and downwards to generate a set of eigenvector pairs. The asymmetric uncertainties, ΔX^+ and ΔX^- , of a quantity X are given by Eq. 6.4 where X_0 is the central prediction, X_k^+ and X_k^- are the predictions using the upwards and downwards variation

of each eigenvector k .

$$\Delta X^+ = \sqrt{\sum_{k=1}^{N_{\text{ev}}} [\max(X_k^+ - X^0, X_k^- - X^0, 0)]^2} \quad (6.4)$$

$$\Delta X^- = \sqrt{\sum_{k=1}^{N_{\text{ev}}} [\min(X_k^+ - X^0, X_k^- - X^0, 0)]^2}$$

The symmetric uncertainty (ΔX^\pm) is given by half the difference of the upwards and downwards variations :

$$\Delta X^\pm = \sqrt{\sum_{k=1}^{N_{\text{ev}}} \left[\frac{X_k^+ - X_k^-}{2} \right]^2} \quad (6.5)$$

The CT10-NLO PDF set uncertainties are downscaled by a factor of 1.64 in order to have the uncertainties at the 68.3% confidence level $\text{CL}(1\sigma)$ instead of 90% $\text{CL}(2\sigma)$ such that to have a uniform treatment with respect to other PDF sets. The PDF uncertainty as derived with the CT10-NLO PDF set is the dominant source of uncertainty and ranges from 3% to 30% for inclusive 2-jet and from 4% to 32% for 3-jet cross-sections. For R_{32} , the ratio of predictions for inclusive 3-jet to that of 2-jet is taken for each eigen vector with upwards and downwards variations separately and then PDF uncertainty is calculated as done for individual cross-sections. The PDF uncertainty ranges and from 2% to 10% for cross-section ratio R_{32} .

6.2.3 Non-perturbative Uncertainty

As discussed in 6.1.2, the differences in the non-perturbative (NP) corrections calculated from various Monte Carlo event generators introduce the NP uncertainty which is of the order of 1% and 1 to 2% for inclusive 2-jet and 3-jet event cross-sections respectively, and < 1% for cross-section ratio R_{32} .

6.2.4 Total Theoretical Uncertainty

The total systematic theoretical uncertainties are obtained as the quadratic sum of the scale, PDF and NP uncertainties. Figure 6.5 presents the systematic theoretical uncertainties affecting the cross-section measurement for inclusive 2-jet (top left) and 3-jet (top right) events and the cross-section ratio R_{32} (bottom), using CT10-NLO PDF set. The scale (red dashed line), PDF (green line) and NP (blue dashed line) uncertainties as well as total theoretical uncertainty (black dashed line) are shown. The total theoretical uncertainty is asymmetric and dominated by PDF uncertainty which grows in magnitude with increasing value of $H_{T,2}/2$. Table 6.2

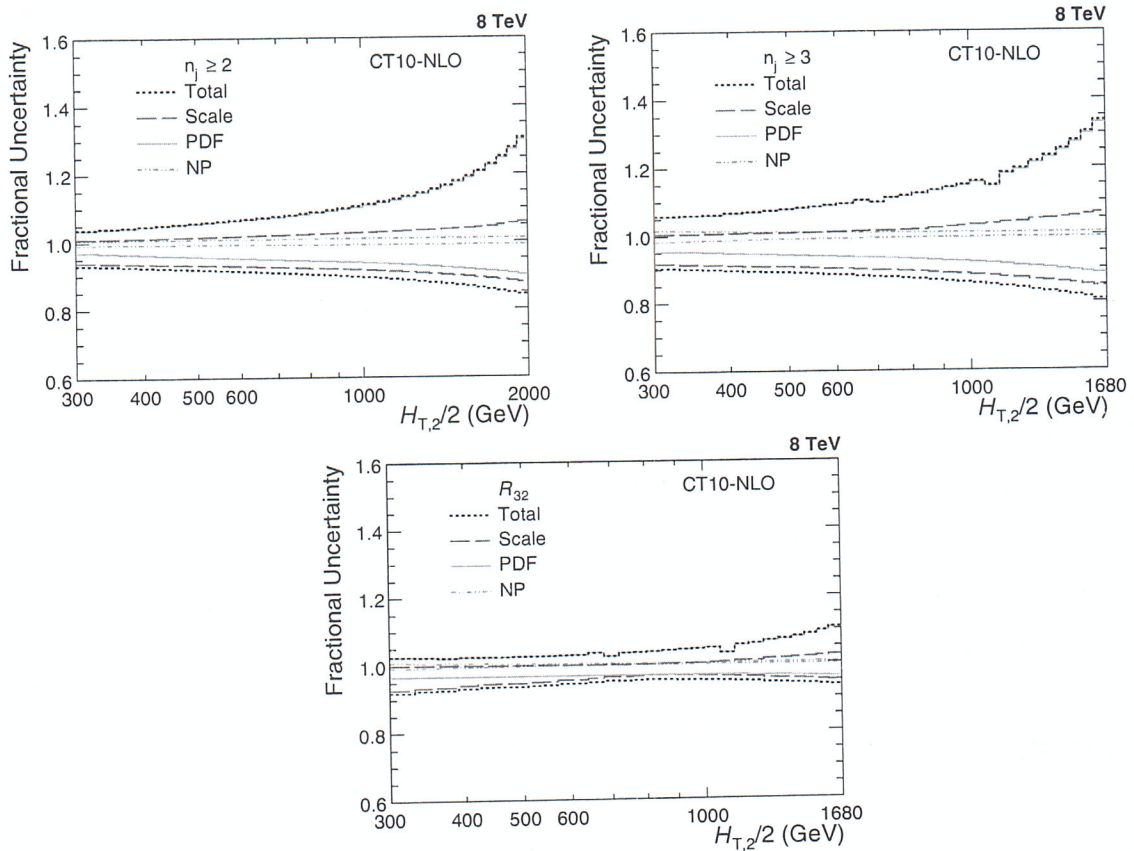


Figure 6.5: The systematic theoretical uncertainties affecting the cross-section measurement for inclusive 2-jet (top left) and 3-jet (top right) events and their ratio R_{32} (bottom). The scale (red dashed line), PDF (green line) and NP (blue dashed line) uncertainties as well as total uncertainty (black dashed line) obtained using line) uncertainties as well as total uncertainty (black dashed line) obtained using CT10-NLO PDF set are shown. The total theoretical uncertainty is asymmetric and dominated by PDF uncertainty.

quotes the values of the theoretical uncertainty from each source as well as total uncertainty affecting the measurements. The bin-wise values of uncertainties (in %) from each source as well as total uncertainty are shown in Tables A.5, A.6 and A.7 for $n_j \geq 2$ and $n_j \geq 3$ event cross-sections and the cross-section ratio R_{32} , respectively. The computation of the NLO predictions with NLOJET++ is also subject to statistical fluctuations from the complex numerical integrations. For the inclusive 2-jet event cross-sections this uncertainty is smaller than about a per mille, while for the inclusive 3-jet event cross-section it amounts to 1-9 per mille. Hence the statistical uncertainty is not considered in the total theoretical uncertainty. The small dips at ~ 700 and 1000 GeV in the PDF uncertainty for inclusive 3-jet events cross-sections and the cross-section ratio R_{32} is a feature of the CT10-NLO PDF set.

Table 6.2: Overview of all systematic theoretical uncertainties, obtained using CT10-NLO PDF set, affecting the measurement of cross-sections for inclusive 2-jet (left) and 3-jet (middle) events and the cross-section ratio R_{32} (right).

Uncertainty Source	Inclusive 2-jet	Inclusive 3-jet	R_{32}
Scale	5 to 13%	11 to 17%	6 to 8%
PDF	3 to 30%	4 to 32%	2 to 10%
Non-perturbative (NP)	1%	1 to 2%	< 1%
Total	3 to 30%	5 to 34%	3 to 11%

It is
considered
in the fits!
It is the only
uncorrelated
source from
theory!

6.3 Comparison of Theory to Data

After correcting the measurement for detector effects as well as NLO pQCD calculations for non-perturbative (NP) and electroweak (EW) effects, it is now feasible to compare the measured cross-sections with the theory predictions. Figure 6.6 shows the measured differential inclusive 2-jet and 3-jet event cross-sections as a function of $H_{T,2}/2$ after unfolding for detector effects. On the left, the measurements (points) are compared to the NLOJET++ predictions using the CT10-NLO PDF set (line),

corrected for NP effects and in addition for EW effects in the 2-jet case. On the right, the comparison is made to the predictions from MADGRAPH5+PYTHIA6 (MG+P6) with tune Z2* (line), corrected for EW effects in the 2-jet case. The error bars give the total experimental uncertainty, given by the quadrature sum of the statistical and systematic uncertainties. On a logarithmic scale, the data are in good agreement with the NLO predictions over the whole range of $H_{T,2}/2$ from 300 GeV up to 2000 (2-jet) and 1680 GeV (3-jet) respectively.

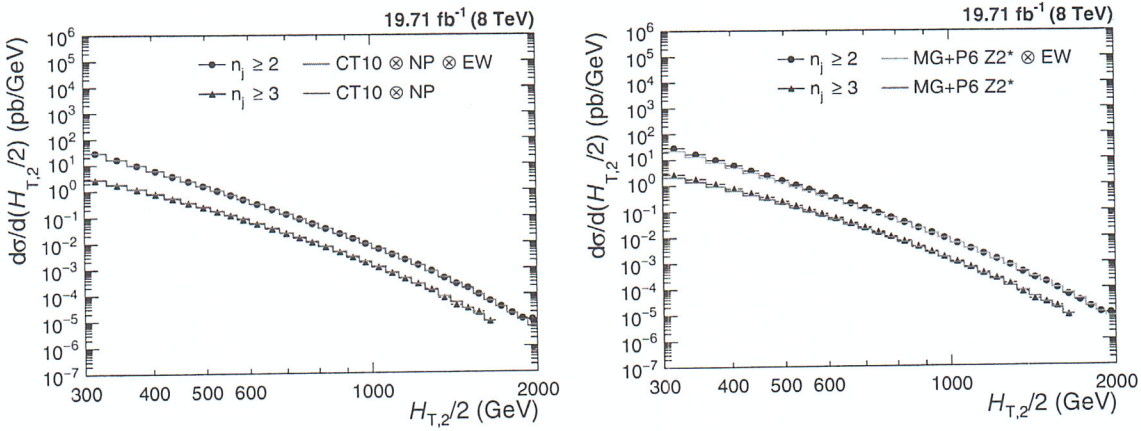


Figure 6.6: Comparison of the measured differential inclusive 2-jet and 3-jet event cross-sections as a function of $H_{T,2}/2$ to theoretical predictions. On the left, the data (points) are shown together with NLOJET++ predictions (line) using the CT10-NLO PDF set, corrected for non-perturbative (NP) and electroweak (EW) effects (2-jet) or only NP effects (3-jet). On the (right), the data (points) are compared to predictions from MADGRAPH5+PYTHIA6 (MG+P6) with tune Z2* (line), corrected for EW effects in the 2-jet case. The error bars give the total experimental uncertainty, given by the quadrature sum of the statistical and systematic uncertainties.

Figure 6.7 shows the cross-section ratio R_{32} obtained from unfolded data (solid circles) in comparison to that from NLO pQCD predictions obtained using the CT10-NLO PDF set corrected with NP corrections (line). The error bars here represent the total experimental uncertainty derived as quadratic sum from all uncertainty sources. The deviations of measured R_{32} from the predicted theoretical value can be explained by the electroweak effects which are not considered yet because of their unavailability for inclusive 3-jet event cross-sections.

For better comparisons, the ratios of the data over the theory at NLO are also shown from CT10!

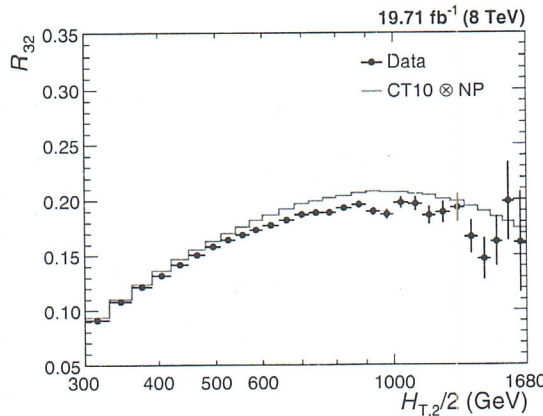


Figure 6.7: Cross-section ratio R_{32} as a function of $H_{T,2}/2$ calculated from data (solid circles) in comparison to that from NLO pQCD predictions obtained using the CT10-NLO PDF set corrected with non-perturbative (NP) corrections (line). The error bars correspond to the total experimental uncertainty derived as quadratic sum from all uncertainty sources.

studied in detail. In Fig. 6.8, the ratios of the data over NLO JET++ predictions using the CT10-NLO PDF set are shown for inclusive 2-jet (top left) and 3-jet (top right) event cross-sections as well as their ratio R_{32} (bottom). The data are well described by the predictions within their uncertainties, which are dominated at large $H_{T,2}/2$ by PDF effects in the upwards and by scale variations in the downwards direction. A trend towards an increasing systematic excess of the 2-jet data with respect to theory, starting at about 1 TeV in $H_{T,2}/2$, is remedied by the inclusion of EWK corrections. In the 3-jet case the statistical precision of the data and the reach in $H_{T,2}/2$ is insufficient to observe any effect. The alternative PDF sets MSTW2008 and NNPDF2.3 exhibit a small underestimation of the cross-sections at high $H_{T,2}/2$.

The POWHEG framework providing the NLO dijet calculation matched to the parton showers of PYTHIA8 employed with the CUETS1 and CUETM1 tunes [78] is also used for a comparison. The ratios of the data w.r.t. theory from POWHEG+PYTHIA8 with tune CUETS1 are shown for inclusive 2-jet (top left) and 3-jet (top right) event cross-sections as well as their ratio R_{32} (bottom) in Fig. 6.9. For comparison, the LO prediction from PYTHIA6 with tune Z2*, the tree-level multi-leg improved prediction by MADGRAPH5+PYTHIA6 with tune Z2*, and the matched

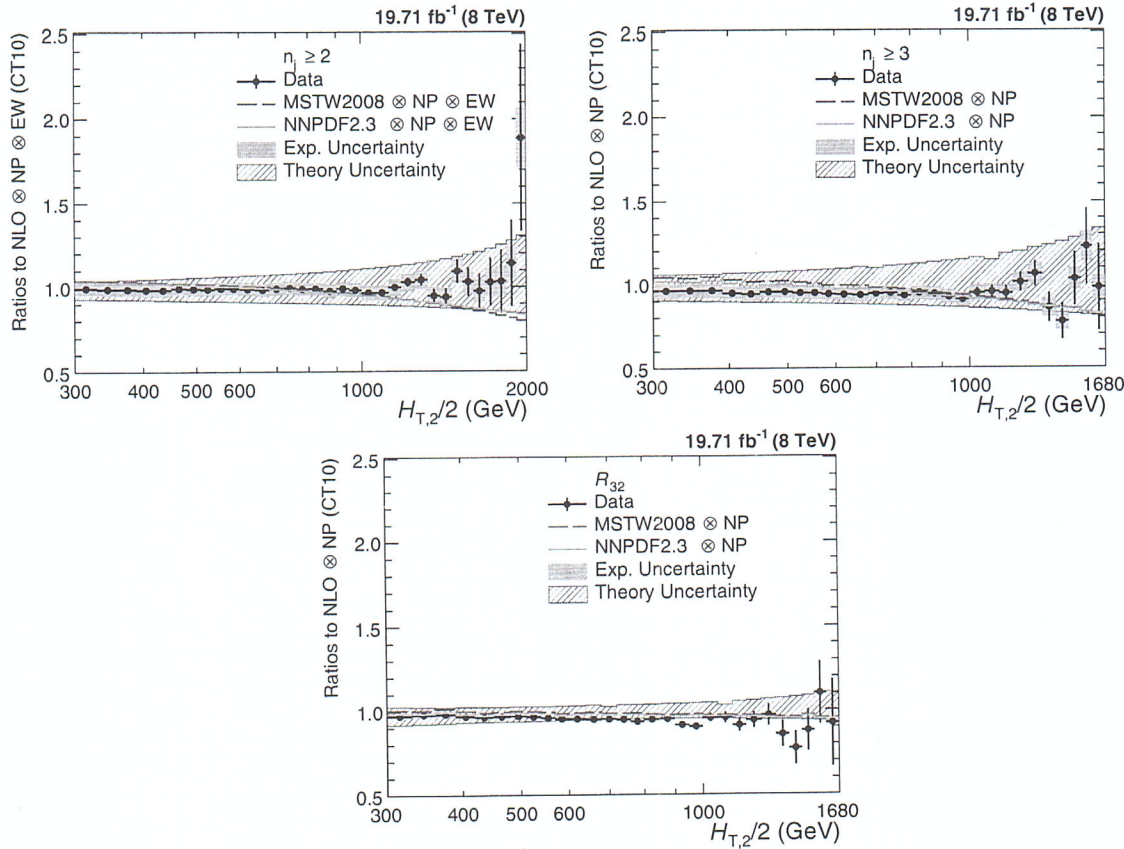


Figure 6.8: Ratio of the data over theory using the CT10-NLO PDF set for inclusive 2-jet (top left) and 3-jet (top right) event cross-sections and their ratio R_{32} (bottom). The theory predictions are corrected for non-perturbative effects (NP) and also for electroweak effects (EW) for inclusive 2-jet only. For comparison predictions employing two other PDF sets, MSTW2008 and NNPDF2.3, are also shown. The error bars represent the statistical uncertainty of the data and the shaded rectangles represents the total experimental systematic uncertainty. The shaded band around unity indicate the total uncertainty of the theory.

NLO prediction from POWHEG+PYTHIA8 with tune CUETM1 are shown as well. EW corrections have been accounted for in this comparison for the 2-jet case only. Significant discrepancies, which are cancelled to a large extent in the ratio R_{32} , are visible in the comparison with the LO prediction from MADGRAPH5+PYTHIA6 with tune Z2*, in particular for small $H_{T,2}/2$. In contrast, the employed dijet MC POWHEG+PYTHIA8 better describe the 2-jet event cross-section, but fail for the 3-jet case.

The jet measurements at hadron colliders can be used to extract the strong coupling constant α_S , which is discussed in the next chapter.

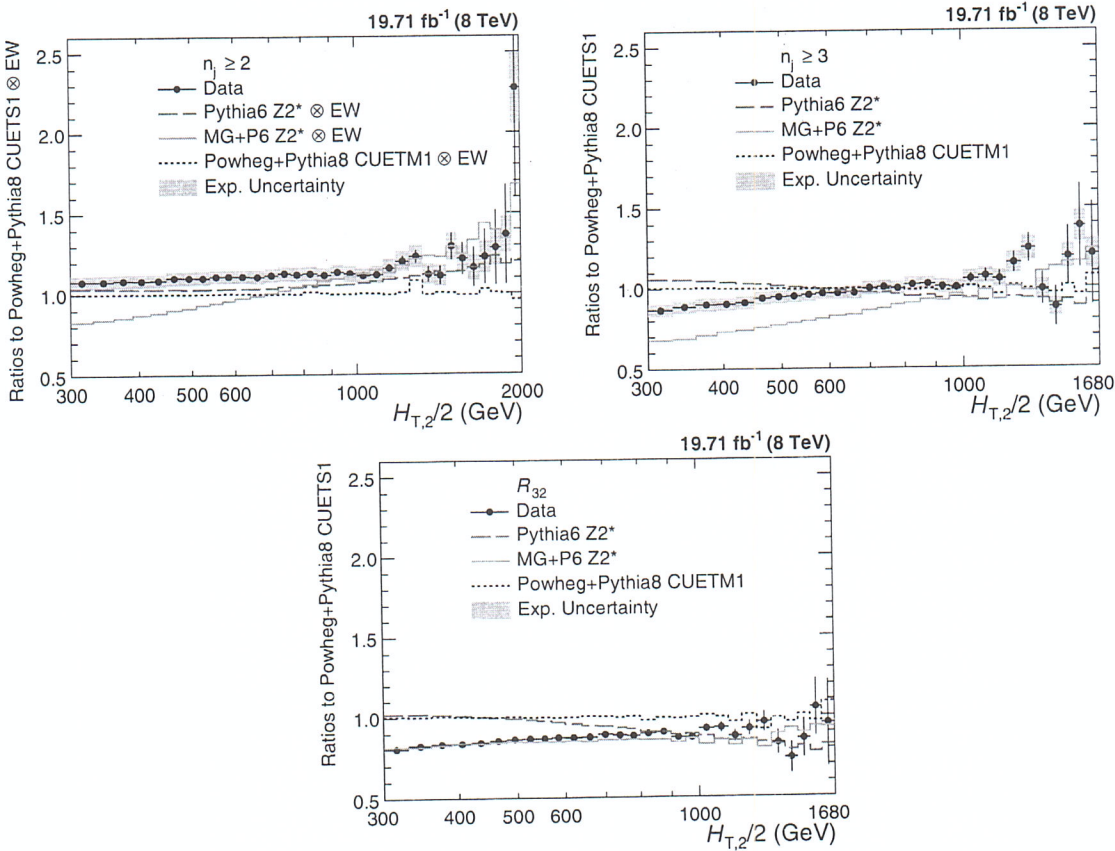


Figure 6.9: Ratio of the data over the predictions from POWHEG+PYTHIA8 with tune CUETS1 are presented for inclusive 2-jet (top left) and 3-jet (top right) event cross-sections as well as their ratio R_{32} (bottom). For comparison the alternative tune CUETM1 of POWHEG+PYTHIA8, the tree-level multi-leg improved prediction by MADGRAPH5+PYTHIA6 with tune $Z2^*$, and the LO MC predictions from PYTHIA6 tune $Z2^*$ are shown as well. The error bars correspond to the statistical uncertainty of the data and the shaded rectangles to the total experimental systematic uncertainty. EW corrections have been accounted for in this comparison for the 2-jet case only.

Chapter 7

Determination of the Strong Coupling Constant

The inclusive jet production cross-section at hadron colliders mainly depends on the strong coupling constant α_S for a given center-of-mass energy. Hence the measurements of the inclusive jet cross-section and jet properties provide a direct probe to measure the strong coupling constant. The measurement of α_S has been already done by various experiments such as CMS [1, 99, 113, 122, 123], ATLAS [124], D0 [125, 126], H1 [127, 128], and ZEUS [129]. In this thesis, the value of the strong coupling constant at the scale of the Z boson mass $\alpha_s(M_Z)$, is extracted using the measurements of differential inclusive 2-jet and 3-jet event cross-sections as well as the cross-section ratio R_{32} , as a function of $H_{\text{T},2}/2$. The differential inclusive jet production cross-section up to NLO is given by [130] :

$$\frac{d\sigma}{d(H_{\text{T},2}/2)} = \alpha_S^2(\mu_r) \hat{X}^{(0)}(\mu_f, H_{\text{T},2}/2) [1 + \alpha_S(\mu_r) K1(\mu_r, \mu_f, H_{\text{T},2}/2)] \quad (7.1)$$

where $\frac{d\sigma}{d(H_{\text{T},2}/2)}$ is the differential inclusive jet production cross-section as a function of $H_{\text{T},2}/2$, μ_r and μ_f are the renormalization and factorization scales set equal to $H_{\text{T},2}/2$, $\alpha_S^2(\mu_r) \hat{X}^{(0)}(\mu_f, H_{\text{T},2}/2)$ is the leading order

(LO) contribution to the differential inclusive jet production cross-section and $\alpha_S^3(\mu_r)\hat{X}^{(0)}(\mu_f, H_{T,2}/2)K1(\mu_r, \mu_f, H_{T,2}/2)$ is the next-to-leading order (NLO) contribution. Equation 7.1 shows how the inclusive jet production cross-section varies with $\alpha_s(\mu_r)$.

7.1 Sensitivity of Measurements to $\alpha_s(M_Z)$

For a fixed choice of μ_r and μ_f , different input values of $\alpha_s(M_Z)$ to a PDF set will lead to different theory predictions for the differential cross-section distribution. This will give an estimate of the sensitivity of the theory predictions to the varying input value of $\alpha_s(M_Z)$. A comparison of the measured spectrum with the theory predictions obtained using all $\alpha_s(M_Z)$ inputs will give a hint of the input value of $\alpha_s(M_Z)$ for which the theory distribution has the closest matching with data. In this section, the sensitivity of the differential inclusive jet event cross-sections and the cross-section ratio, R_{32} to varying input values of $\alpha_s(M_Z)$ for different PDF sets is demonstrated by plotting the ratios of the data over theory predictions with central value of $\alpha_s(M_Z)$.

Figures 7.1, 7.2 and 7.3 present the ratio of the data to the theory predictions, corrected for NP effects, for all variations in $\alpha_s(M_Z)$ available for the PDF sets CT10, CT14, MSTW2008, MMHT2014 and NNPDF2.3 at NLO evolution order as specified in Table 6.1, for inclusive 2-jet event cross-sections, inclusive 3-jet events cross-sections and ratio R_{32} respectively. The $\alpha_s(M_Z)$ value is varied in the range 0.112-0.127, 0.111-123, 0.110-0.130, 0.108-0.128 and 0.114-0.124 in steps of 0.001 for the CT10, CT14, MSTW2008, MMHT2014 and NNPDF2.3PDF sets, respectively. The error bars correspond to the total experimental uncertainty derived as quadratic sum from all uncertainty sources. The theory predictions are also corrected for EW effects for inclusive 2-jet events cross-section. A small slope increasing with $H_{T,2}/2$ is visible for most PDFs in both cross-sections. This effect is largely cancelled in

the cross-section ratio. R_{32} exhibits a flat behaviour with respect to the predictions for all five PDF sets in the whole range of $H_{T,2}/2$ up to 1680 GeV. Therefore, these data can be used to determine the strong coupling constant, although only up to 1 TeV for the cross-sections as long as electroweak corrections are not taken into account.

Moreover, in Figs. 7.1–7.3, the different sensitivity to $\alpha_s(M_Z)$ caused by the leading power in α_S in the expansion of the 2-jet inclusive ($\propto \alpha_S^2$) and the 3-jet inclusive ($\propto \alpha_S^3$) cross-sections, and their ratio ($\propto \alpha_S^1$), is clearly visible from the spread between the calculations for the smallest and largest value of $\alpha_s(M_Z)$ within the same PDF set. This also demonstrates the potential of cross-section ratios R_{mn} with $(m-n) > 1$.

7.2 Determination of $\alpha_s(M_Z)$

As discussed in the previous section, the measured inclusive 2-jet and 3-jet event cross-sections and their ratio R_{32} can be used for a determination of the strong coupling constant $\alpha_s(M_Z)$. To extract the value of $\alpha_s(M_Z)$, a general fit procedure [1, 99, 123] has been followed as described in the following section.

7.2.1 Fitting Procedure

The value of $\alpha_s(M_Z)$ is determined by minimizing the chi-square (χ^2) between the experimental measurements and the theoretical predictions. The χ^2 is given by the following equation :

$$\chi^2 = M^T C^{-1} M \quad (7.2)$$

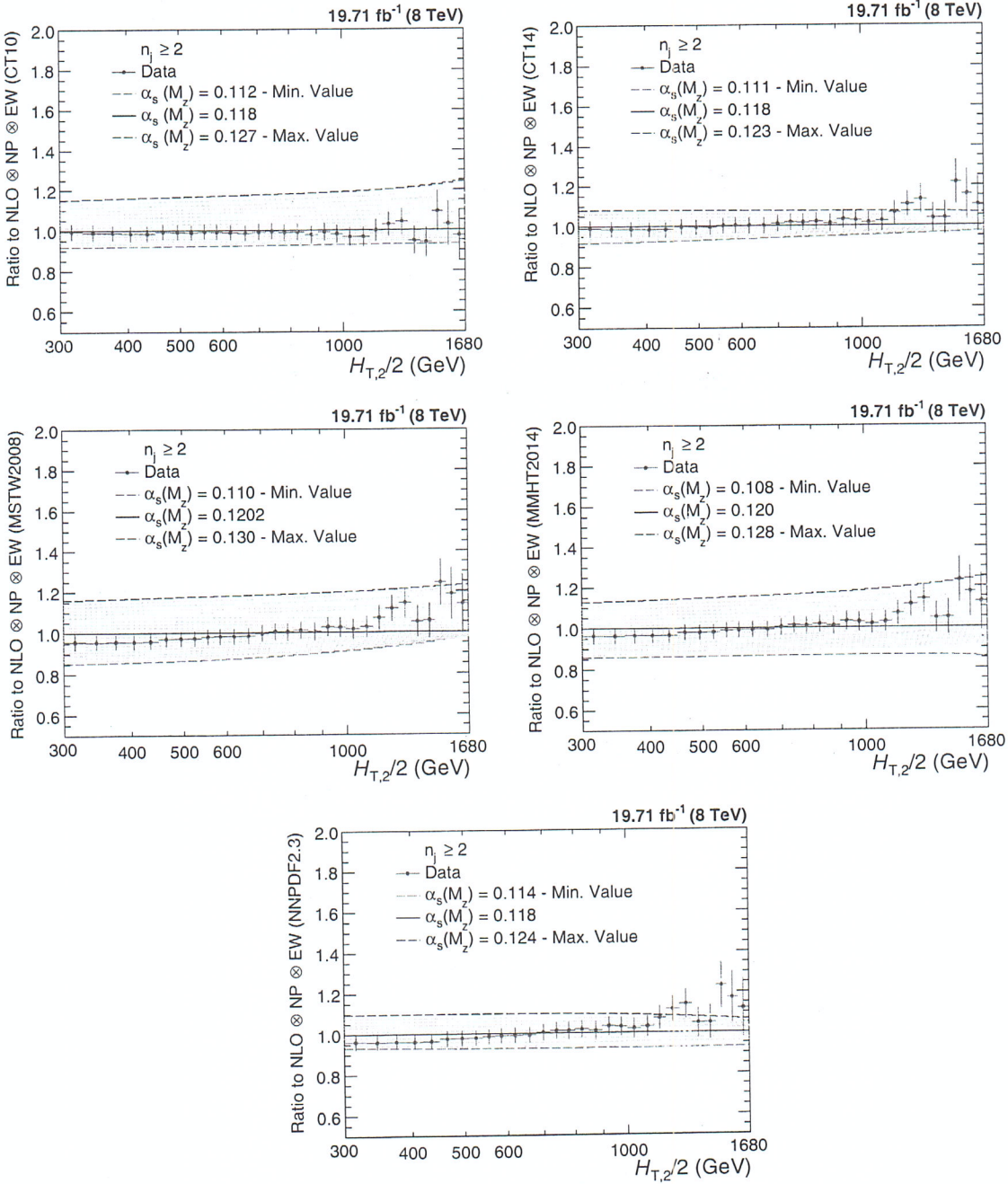


Figure 7.1: Ratio of the measured inclusive 2-jet differential cross-section to theory predictions using the CT10 (top left), the CT14 (top right), the MSTW2008 (middle left), the MMHT2014 (middle right) and NNPDF2.3 (bottom) NLO PDF sets for a series of values of $\alpha_s(M_Z)$. The $\alpha_s(M_Z)$ value is varied in the range 0.112-0.127, 0.111-1.23, 0.110-0.130, 0.108-0.128 and 0.114-0.124 in steps of 0.001 for the CT10, CT14, MSTW2008, MMHT2014 and NNPDF2.3 NLO PDF sets, respectively. The theory predictions are corrected for non-perturbative (NP) and electroweak (EW) effects. The error bars correspond to the total experimental uncertainty.

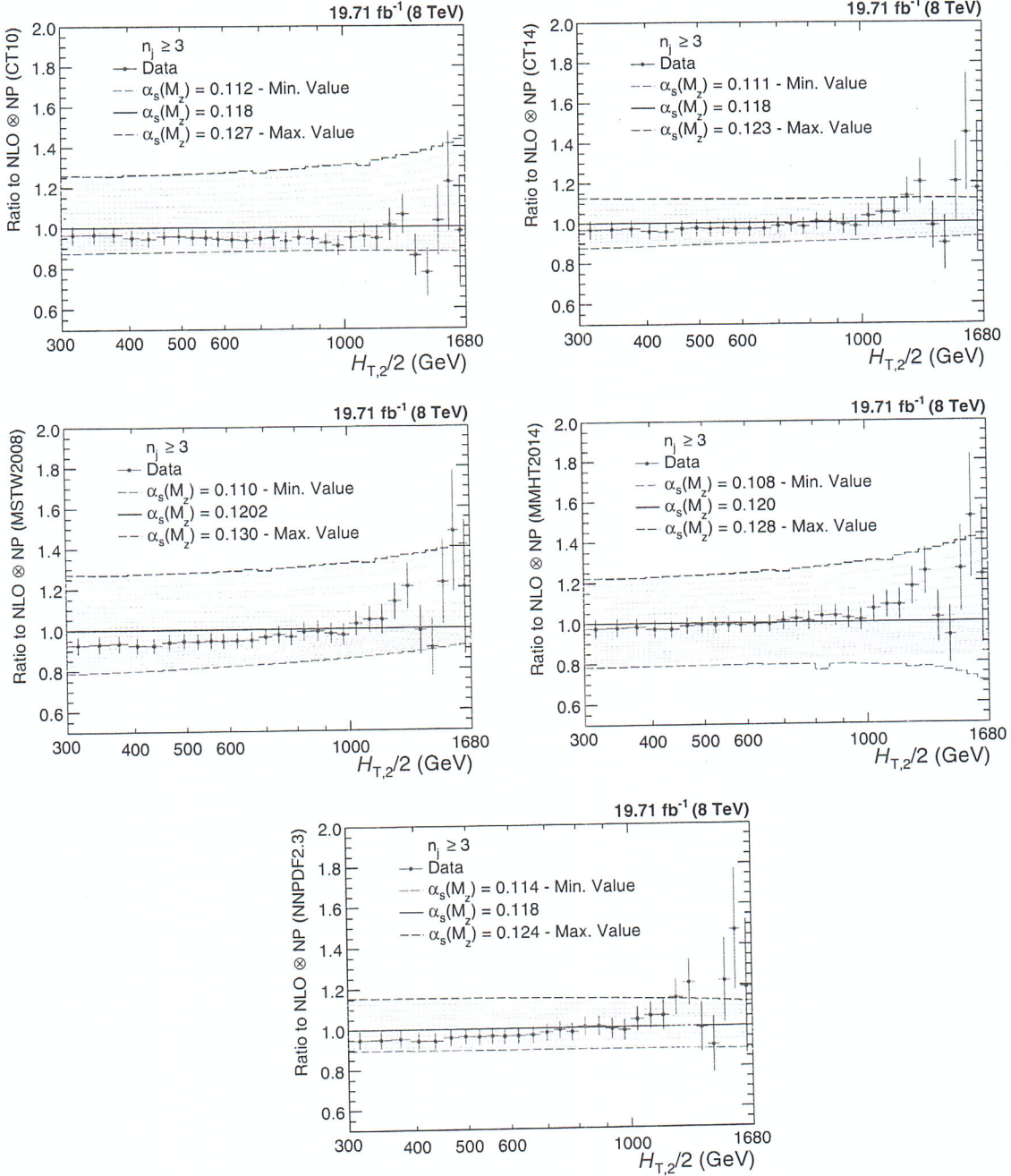


Figure 7.2: Ratio of the measured inclusive 3-jet differential cross-section to theory using the CT10 (top left), the CT14 (top right), the MSTW2008 (middle left), the MMHT2014 (middle right) and NNPDF2.3 (bottom) NLO PDF sets for $\alpha_s(M_Z)$. The $\alpha_s(M_Z)$ value is varied in the range 0.112-0.127, a series of values of $\alpha_s(M_Z)$ are used: 0.112-0.127 for the CT10, 0.111-0.123, 0.110-0.130, 0.108-0.128 and 0.114-0.124 in steps of 0.001 for the CT14, MSTW2008, MMHT2014 and NNPDF2.3 NLO PDF sets, respectively. The theory predictions error bars correspond to the total experimental uncertainty. The theory predictions are corrected for non-perturbative (NP) effects.

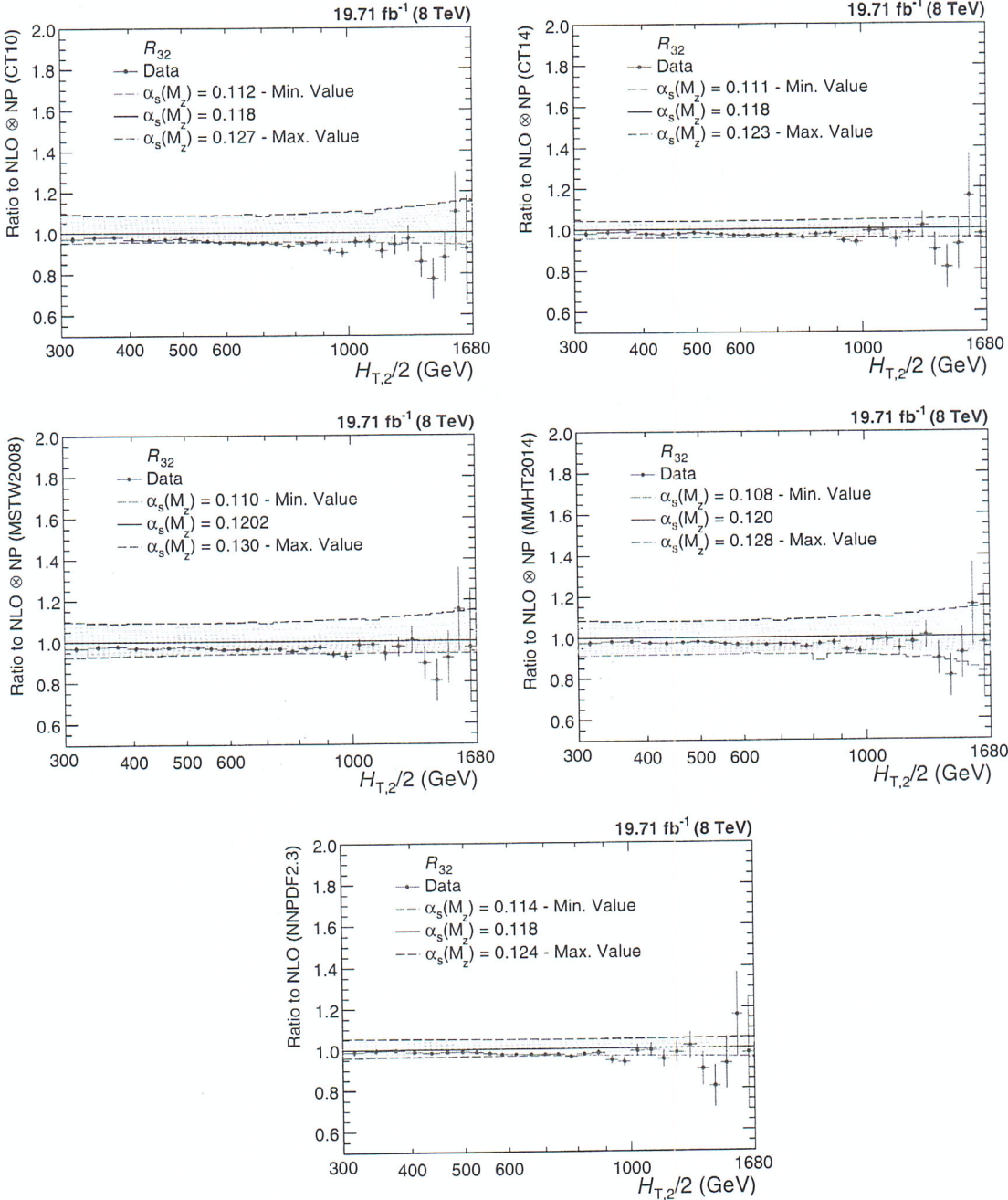


Figure 7.3: Ratio of the measured cross-section ratio, R_{32} to theory predictions using the CT10 (top left), the CT14 (top right), the MSTW2008 (middle left), the MMHT2014 (middle right) and NNPDF2.3 (bottom) NLO PDF sets for a series of values of $\alpha_s(M_Z)$. The $\alpha_s(M_Z)$ value is varied in the range 0.112-0.127, 0.111-1.23, 0.110-0.130, 0.108-0.128 and 0.114-0.124 in steps of 0.001 for the CT10, CT14, MSTW2008, MMHT2014 and NNPDF2.3 NLO PDF sets, respectively. The error bars correspond to the total experimental uncertainty. The theory predictions are corrected for non-perturbative (NP) effects.

where M is the vector of the differences between the data (D^i) and the theoretical values (T^i) in each bin i ,

$$M^i = D^i - T^i \quad (7.3)$$

and C is the covariance matrix including all experimental uncertainties as described in Sec. 5.6 and some theoretical uncertainties discussed in Sec. 6.2. The covariance matrix $C = C_{\text{exp}} + C_{\text{theo}}$ is defined as the sum of covariances of experimental and theoretical sources of uncertainty as follows :

$$C_{\text{exp}} = \text{Cov}^{\text{ExpStat}} + \sum \text{Cov}^{\text{JEC}} + \text{Cov}^{\text{Unfolding}} + \text{Cov}^{\text{Lumi}} + \text{Cov}^{\text{Residual}} \quad (7.4)$$

$$C_{\text{theo}} = \text{Cov}^{\text{TheoStat}} + \text{Cov}^{\text{NP}} + \text{Cov}^{\text{PDF}} \quad (7.5)$$

where the labelled covariance matrices account for the following effects:

- $\text{Cov}^{\text{ExpStat}}$: statistical uncertainty of the data including correlations introduced by the unfolding.
- Cov^{JEC} : the jet energy corrections (JEC) systematic uncertainty.
- $\text{Cov}^{\text{Unfolding}}$: the unfolding systematic uncertainty including the resolution (JER) and model dependence.
- Cov^{Lumi} : the luminosity uncertainty.
- $\text{Cov}^{\text{Residual}}$: a residual uncorrelated systematic uncertainty summarizing individual causes such as small trigger and identification inefficiencies, time dependence of the jet p_T resolution, and uncertainty on the trigger prescale factors.
- $\text{Cov}^{\text{TheoStat}}$: statistical uncertainty caused by numerical integrations in the cross-section computations.

- Cov^{NP} : the systematic uncertainty of the non-perturbative (NP) corrections.
- Cov^{PDF} : the PDF uncertainties.

While taking the differences between theory and data, the treatment of experimental and theoretical systematic uncertainties is crucial. The Unfolding, JEC, Lumi, and PDF and NP systematic uncertainties are treated as 100% correlated among $H_{T,2}/2$ bins. If δ_i is the total uncertainty on the differential cross-section, for the i -th $H_{T,2}/2$ bin, for any of these fully correlated sources, then the (i,j) -th element of the corresponding covariance matrix is given by $\text{COV}_{ij} = \delta_i \times \delta_j$. The JEC, unfolding, and luminosity uncertainties are treated as multiplicative to avoid the statistical bias that arises when estimating uncertainties from data. In fits of the ratio R_{32} , the luminosity and residual uncorrelated uncertainties cancel completely. Partial cancellations between the other sources of uncertainty are taken into account in the fit.

The evaluation of PDF uncertainty depends on the individual PDF set as already discussed in Sec. 6.2.2. The PDF covariance matrix construction varies among different PDF sets. The CT10, CT14, MMHT2014 and MSTW2008 NLO PDF sets employ the eigenvector method to evaluate the PDF uncertainties as explained in Sec. 6.2.2. The number of eigenvectors (N_{ev}) with two PDF members per eigenvector for CT10, CT14, MMHT2014 and MSTW2008 NLO PDF sets are 26, 28, 25 and 20, respectively. The NNPDF2.3 PDF set comes with hundred different replicas (N_{rep}) instead of different eigenvectors, as for CT10 or CT14 PDF sets. The mean uncertainty is calculated as average uncertainty from 100 different replicas. Following the prescription given in [131], the PDF uncertainty is calculated as :

$$(\Delta X)^2 = \frac{1}{N_{\text{rep}} - 1} \sum_{k=1}^{N_{\text{rep}}} [X_k - \langle X_k \rangle]^2 \quad (7.6)$$

where ΔX is the uncertainty on predicted differential cross-section, X_k is the differ-

ential cross-section for k -th replica and $\langle X_k \rangle$ is the average differential cross-section from all the replicas.

Scale uncertainties of the pQCD predictions are taken into account by employing the offset method, i.e. by performing separate fits with varying scale factors as described in the Sec. 6.2.1. The largest upwards and downwards deviations from the default factors are defined as the uncertainty. At NLO such scale variations predominantly lead to smaller cross-sections and also a smaller ratio R_{32} as visible in Fig. 6.5. As a consequence the scale uncertainty in fits is equally asymmetric, where smaller cross-sections or ratios are compensated by an increase in the fitted value for $\alpha_s(M_Z)$.

7.2.2 Fit Results

To determine the value of the strong coupling constant at the scale of the Z boson mass $\alpha_s(M_Z)$, fits to the differential inclusive 2-jet and 3-jet events cross-sections are performed using five different NLO PDF sets : CT10, CT14, MSTW2008, MMHT2014 and NNPDF2.3. The range in $H_{T,2}/2$ is restricted to be between 300 GeV and 1 TeV to avoid the region close to the minimal p_T threshold of 150 GeV for each jet at low p_T and the onset of electroweak effects at high $H_{T,2}/2$, which are available for the dijet case only. The $\alpha_s(M_Z)$ results obtained from a simultaneous fit to all 19 $H_{T,2}/2$ bins in the above mentioned range are reported in Table 7.1. For comparison, a simultaneous fit to both cross-sections ignoring any correlations, and a fit to the cross-section ratio R_{32} , fully accounting for correlations is also performed and the results are tabulated in Table 7.2. The electroweak effects are assumed to cancel in the ratio as do the luminosity and the uncorrelated uncertainty.

All cross-section fits give compatible values for $\alpha_s(M_Z)$ in the range of 0.115–0.118 whereas for the ratio R_{32} somewhat smaller values are obtained. But for individual cross-sections, χ^2/n_{dof} values are small as compared to the cross-section

ratio R_{32} . A possible explanation is an overestimation of the residual uncorrelated uncertainty of 1% that is cancelled for R_{32} . If the fits are repeated with an assumed uncertainty of 0.25% instead, the χ^2/n_{dof} values lie around unity while the $\alpha_s(M_Z)$ values are still compatible with the previous results but with slightly reduced uncertainties.

Table 7.1: Determination of $\alpha_s(M_Z)$ from the inclusive 2-jet and 3-jet event cross-sections using five PDF sets at NLO. Only total uncertainties without scale variations are quoted. The results are obtained from a simultaneous fit to all 19 $H_{\text{T},2}/2$ bins in the restricted range of $300 < H_{\text{T},2}/2 < 1000$ GeV.

PDF set	Inclusive 2-jets			Inclusive 3-jets		
	$\alpha_s(M_Z)$	$\pm \Delta \alpha_s(M_Z)$	χ^2/n_{dof}	$\alpha_s(M_Z)$	$\pm \Delta \alpha_s(M_Z)$	χ^2/n_{dof}
CT10	0.1174	0.0032	3.0/18	0.1169	0.0027	5.4/18
CT14	0.1160	0.0035	3.5/18	0.1159	0.0031	6.1/18
MSTW2008	0.1159	0.0025	5.3/18	0.1161	0.0021	6.7/18
MMHT2014	0.1165	0.0034	5.9/18	0.1166	0.0025	7.1/18
NNPDF2.3	0.1183	0.0025	9.7/18	0.1179	0.0021	9.1/18

Table 7.2: Determination of $\alpha_s(M_Z)$ from the inclusive 2-jet and 3-jet event cross-sections simultaneously and from their ratio R_{32} using five PDF sets at NLO. Only total uncertainties without scale variations are quoted. The results are obtained from a simultaneous fit to all 38 (left) and 19 (right) $H_{\text{T},2}/2$ bins in the restricted range of $300 < H_{\text{T},2}/2 < 1000$ GeV. For comparison, correlations between the two cross-sections are neglected in the simultaneous fit on the left, but fully taken into account in the ratio fit on the right.

PDF set	Inclusive 2- and 3-jets			R_{32}		
	$\alpha_s(M_Z)$	$\pm \Delta \alpha_s(M_Z)$	χ^2/n_{dof}	$\alpha_s(M_Z)$	$\pm \Delta \alpha_s(M_Z)$	χ^2/n_{dof}
CT10	0.1170	0.0026	8.2/37	0.1141	0.0028	19./18
CT14	0.1161	0.0029	9.1/37	0.1139	0.0032	15./18
MSTW2008	0.1161	0.0021	11./37	0.1150	0.0023	21./18
MMHT2014	0.1168	0.0025	11./37	0.1142	0.0022	19./18
NNPDF2.3	0.1188	0.0019	15./37	0.1184	0.0021	12./18

To investigate how the electroweak (EW) corrections affect the fit results for $\alpha_s(M_Z)$, the range in $H_{\text{T},2}/2$ is extended to $300 < H_{\text{T},2}/2 < 1680$ GeV. $\alpha_s(M_Z)$ values are obtained from fits to the inclusive 2-jet event cross-section in this range with or without EW correction factors and the results are presented in Table 7.3. The largest impact is a reduction in χ^2/n_{dof} , which indicates a better agreement

when EW effects are included. In addition, a tendency to slightly smaller $\alpha_s(M_Z)$ values is observed without the EW corrections. For the ratio R_{32} , it is expected that these effects are much reduced.

Table 7.3: Determination of $\alpha_s(M_Z)$ from the inclusive 2-jet event cross-section using five PDF sets at NLO without (left) and with (right) electroweak (EW) corrections. Only total uncertainties without scale variations are quoted. The results are obtained from a simultaneous fit to all 29 $H_{T,2}/2$ bins in the range of $300 < H_{T,2}/2 < 1680$ GeV.

PDF set	without EW			with EW		
	$\alpha_s(M_Z)$	$\pm \Delta \alpha_s(M_Z)$	χ^2/n_{dof}	$\alpha_s(M_Z)$	$\pm \Delta \alpha_s(M_Z)$	χ^2/n_{dof}
CT10	0.1163	0.0034	15./28	0.1165	0.0032	14./28
CT14	0.1137	0.0033	24./28	0.1144	0.0033	17./28
MSTW2008	0.1093	0.0028	27./28	0.1133	0.0023	19./28
MMHT2014	0.1127	0.0032	32./28	0.1141	0.0032	21./28
NNPDF2.3	0.1162	0.0024	31./28	0.1168	0.0024	23./28

From Fig. 7.3 follows that only the PDF sets MSTW2008 and MMHT2014 provide a large enough range in $\alpha_s(M_Z)$ values to ensure fits without extrapolation. The other three PDF sets are at the limit such that reliable fits cannot be performed for all scale settings and/or bins in scale $Q = H_{T,2}/2$. Since many systematic uncertainties cancel completely or partially in the cross-section ratio R_{32} as compared to the individual cross-sections, R_{32} is used mainly to determine the value of $\alpha_s(M_Z)$. Table 7.4 gives the complete results for MSTW2008 and MMHT2014 for the full range in $H_{T,2}/2$ of 300 GeV up to 1.68 TeV along with the corresponding components of PDF, scale, NP and total experimental except scale uncertainties. In contrast to fits at NLO using cross-sections where the scale uncertainty recipe usually leads to a very asymmetric behaviour with larger downward uncertainties in the case, this is inverted for the fits to the cross-section ratio R_{32} . The scale uncertainty is the most dominant source of total uncertainty on $\alpha_s(M_Z)$. These values are determined with the central renormalization and factorization scales i.e. $\mu_r = \mu_f = H_{T,2}/2$. The values are also determined for the six scale factor combinations for the two PDF sets MSTW2008 and MMHT2014 and the results are shown in Table 7.5.

The uncertainty decomposition for $\alpha_s(M_Z)$ determined from cross-section ratio R_{32} is performed in four sub-ranges of $H_{T,2}/2$ and the results are shown in Table 7.6. The statistical uncertainty of the NLO computation is negligible in comparison to any of the other sources of uncertainty. Electroweak corrections, significant only at high $H_{T,2}/2$, are assumed to cancel between the numerator and denominator.

Finally, the values of the strong coupling constant at the scale of mass of Z boson $\alpha_s(M_Z)$, determined from the ratio R_{32} using the two most compatible PDF sets, are :

- Using the MSTW2008 PDF set, which dates from before the LHC start :

$$\begin{aligned} \alpha_s(M_Z) &= 0.1150 \pm 0.0010 \text{ (exp)} \pm 0.0013 \text{ (PDF)} \pm 0.0015 \text{ (NP)} {}^{+0.0050}_{-0.0000} \text{ (scale)} \\ &= 0.1150 \pm 0.0023 \text{ (all except scale)} {}^{+0.0050}_{-0.0000} \text{ (scale)} \end{aligned} \quad (7.7)$$

- Using the MMHT2014 PDF set, which uses the LHC jet data to determine the PDF parameters :

$$\begin{aligned} \alpha_s(M_Z) &= 0.1142 \pm 0.0010 \text{ (exp)} \pm 0.0013 \text{ (PDF)} \pm 0.0014 \text{ (NP)} {}^{+0.0049}_{-0.0006} \text{ (scale)} \\ &= 0.1142 \pm 0.0022 \text{ (all except scale)} {}^{+0.0049}_{-0.0006} \text{ (scale)} \end{aligned} \quad (7.8)$$

7.3 Running of the Strong Coupling Constant

The value of the strong coupling constant α_s depends on the energy scale Q and it decreases with the increase of scale Q . To study this dependence, the determination of α_s is carried out at different energies. The procedure to extract $\alpha_s(Q)$ is same as the one followed for the $\alpha_s(M_Z)$. To have different energy scales, the fitted $H_{T,2}/2$

Table 7.4: Determination of $\alpha_s(M_Z)$ from the ratio R_{32} using the two most compatible PDF sets MSTW2008 and MMHT2014 at NLO along with the corresponding components of PDF, scale, NP and total (except scale) experimental uncertainties. The results are obtained from a simultaneous fit to all 29 $H_{T,2}/2$ bins in the full range of $300 < H_{T,2}/2 < 1680$ GeV.

PDF set	$\alpha_s(M_Z)$	exp	PDF	NP	all exc.	scale	χ^2/n_{dof}
MSTW2008	0.1150	± 0.0010	± 0.0013	± 0.0015	± 0.0023	$^{+0.0050}_{-0.0000}$	26./28
MMHT2014	0.1142	± 0.0010	± 0.0013	± 0.0014	± 0.0022	$^{+0.0049}_{-0.0006}$	24./28

Table 7.5: Determination of $\alpha_s(M_Z)$ from the ratio R_{32} in the $H_{T,2}/2$ range from 300 up to 1680 GeV at the central scale and for the six scale factor combinations for the two PDF sets MSTW2008 and MMHT2014.

$\mu_r/H_{T,2}/2$	$\mu_f/H_{T,2}/2$	MSTW2008		MMHT2014	
		$\alpha_s(M_Z)$	χ^2/n_{dof}	$\alpha_s(M_Z)$	χ^2/n_{dof}
1	1	0.1150	26./28	0.1142	24./28
1/2	1/2	0.1165	77./28	0.1160	73./28
2	2	0.1200	18./28	0.1191	18./28
1/2	1	0.1150	53./28	0.1136	48./28
1	1/2	0.1150	30./28	0.1142	28./28
1	2	0.1155	23./28	0.1147	22./28
2	1	0.1180	19./28	0.1175	19./28

Table 7.6: Uncertainty decomposition for $\alpha_s(M_Z)$ from the determination of α_S from the jet event rate R_{32} in bins of $H_{T,2}/2$. The statistical uncertainty of the NLO computation is negligible in comparison to any of the other sources of uncertainty. Electroweak corrections, significant only at high $H_{T,2}/2$, are assumed to cancel between the numerator and denominator.

$H_{T,2}/2$ (GeV)	MSTW2008					MMHT2014				
	$\alpha_s(M_Z)$	exp	PDF	NP	scale	$\alpha_s(M_Z)$	exp	PDF	NP	scale
300-420	0.1157	± 0.0015	± 0.0014	± 0.0019	$^{+0.0053}_{-0.0000}$	0.1158	± 0.0014	± 0.0010	± 0.0019	$^{+0.0052}_{-0.0000}$
420-600	0.1153	± 0.0011	± 0.0014	± 0.0018	$^{+0.0057}_{-0.0000}$	0.1154	± 0.0011	± 0.0012	± 0.0017	$^{+0.0056}_{-0.0000}$
600-1000	0.1134	± 0.0013	± 0.0016	± 0.0019	$^{+0.0052}_{-0.0000}$	0.1140	± 0.0012	± 0.0012	± 0.0018	$^{+0.0045}_{-0.0000}$
1000-1680	0.1147	± 0.0029	± 0.0017	± 0.0018	$^{+0.0063}_{-0.0011}$	0.1154	± 0.0025	± 0.0014	± 0.0015	$^{+0.0056}_{-0.0011}$
300-1680	0.1150	± 0.0010	± 0.0013	± 0.0015	$^{+0.0050}_{-0.0000}$	0.1142	± 0.0010	± 0.0013	± 0.0014	$^{+0.0049}_{-0.0006}$

range 300 - 1680 GeV is divided into four different sub-ranges as shown by the first column in Table 7.7. Each of the $H_{T,2}/2$ range is associated with a scale Q , which is the differential cross-section weighted average $H_{T,2}/2$ scale from the inclusive 2-jet calculations and integrated over all the measured $H_{T,2}/2$ bins contributing to that given $H_{T,2}/2$ range. Let N_{bin}^j be the total number of measured $H_{T,2}/2$ bins contributing to the j -th $H_{T,2}/2$ range, then the corresponding scale Q_j , shown in second column of Table 7.7, is calculated as :

$$Q_j = \frac{\sum_{i=1}^{N_{bin}^j} H_{T,2}^i \left[\frac{d\sigma}{d(H_{T,2}/2)} \right]^i}{\sum_{i=1}^{N_{bin}^j} \left[\frac{d\sigma}{d(H_{T,2}/2)} \right]^i} \quad (7.9)$$

The value of $\alpha_s(M_Z)$ is extracted in each $H_{T,2}/2$ range. These extracted $\alpha_s(M_Z)$ values are evolved to the corresponding values $\alpha_s(Q)$ and are quoted in Table 7.7 along with the extracted $\alpha_s(M_Z)$ values and the total uncertainty. The evolution is performed for five flavours at 2-loop order with the RUNDEC program [132, 133]. The obtained $\alpha_s(Q)$ points (black solid circles) are shown as a function of scale Q in Fig. 7.4. The black solid line and the yellow uncertainty band are evolved using $\alpha_s(M_Z) = 0.1150 \pm 0.0023$ (all except scale) $^{+0.0050}_{-0.0000}$ (scale) obtained using MSTW2008 NLO PDF set. The world average [21] (dashed line) and results from other measurements of the CMS [1, 99, 113, 122, 123], ATLAS [124], D0 [125, 126], H1 [127, 128], and ZEUS [129] experiments are also imposed. The current measurement is in very good agreement within the uncertainty with other results obtained by previous experiments as well as with the world average value of $\alpha_s(M_Z) = 0.1181 \pm 0.0011$ derived in Ref. [21].

Table 7.7: Evolution of the strong coupling constant between the scale of the Z boson mass and the cross-section averaged $H_{T,2}/2$ scale $\langle Q \rangle$ for the separate determinations in each respective fit range. The evolution is performed for five flavours at 2-loop order with the RUNDEC program [132, 133].

$H_{T,2}/2$ (GeV)	$\langle Q \rangle$ (GeV)	$\alpha_s(M_Z)$	$\alpha_s(Q)$	No. of data points	χ^2/n_{dof}
300-420	340	$0.1157^{+0.0060}_{-0.0030}$	$0.0969^{+0.0041}_{-0.0021}$	4	2.8/3
420-600	476	$0.1153^{+0.0062}_{-0.0025}$	$0.0928^{+0.0039}_{-0.0016}$	6	6.1/5
600-1000	685	$0.1134^{+0.0059}_{-0.0028}$	$0.0879^{+0.0035}_{-0.0017}$	9	7.1/8
1000-1680	1114	$0.1147^{+0.0074}_{-0.0040}$	$0.0841^{+0.0039}_{-0.0021}$	10	5.4/9

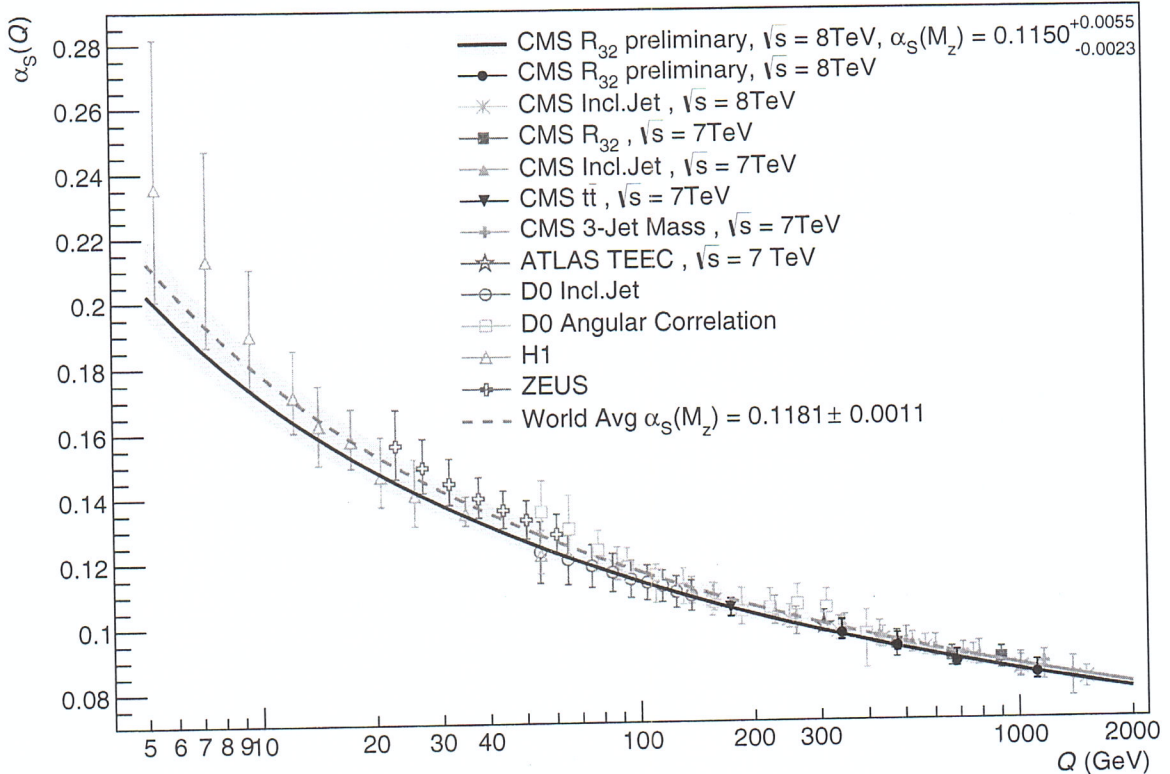


Figure 7.4: The running $\alpha_s(Q)$ as a function of the energy scale Q is shown as obtained by using the MSTW2008 NLO PDF set. The solid line and the uncertainty band are drawn by evolving the extracted $\alpha_s(M_Z)$ values using the 2-loop 5-flavour renormalization group equations as implemented in RUNDEC [132, 133]. The dashed line represents the evolution of the world average [21] and the black circles correspond to the $\alpha_s(Q)$ determinations presented in Table 7.7. Results from other measurements of CMS [1, 99, 113, 122, 123], ATLAS [124], D0 [125, 126], H1 [127, 128], and ZEUS [129] are superimposed.

Chapter 8

Summary

Inclusive multijet production cross-section measured precisely in terms of jet transverse momentum is one of the important observables in understanding physics at hadron colliders. It provides the essential information about the structure of parton through parton distribution functions (PDFs) and the precise measurement of the strong coupling constant α_s . The value of the strong coupling constant at the scale of the Z boson mass $\alpha_s(M_Z)$ can be determined using cross-section ratio instead of individual cross-sections because many uncertainties of theoretical and experimental origin cancel in the ratio which reduces the dependence on PDFs, renormalization and factorization scales, luminosity etc.

In this thesis, a measurement of the inclusive 2-jet and 3-jet event cross-sections as well as the cross-section ratio R_{32} has been presented. The data sample has been collected from proton-proton collisions recorded with the CMS detector at a centre-of-mass energy of 8 TeV and corresponds to an integrated luminosity of 19.7 fb^{-1} . The jets are reconstructed with the anti- k_t clustering algorithm for a jet size parameter $R = 0.7$. The inclusive 2-jet and 3-jet event cross-sections are measured differentially as a function of the average transverse momentum of the two leading jets, referred as $H_{\text{T},2}/2$. The ratio R_{32} is obtained by dividing the differential cross-sections of inclusive 3-jet events to that of inclusive 2-jet one in

Physical review

each bin of $H_{T,2}/2$. An appropriate selection criteria has been designed for choosing the best events for analysis. The measurements are performed at a central rapidity of $|y| < 2.5$ in a range of $300 < H_{T,2}/2 < 2000$ GeV for inclusive 2-jet event cross-sections and $300 < H_{T,2}/2 < 1680$ GeV for inclusive 3-jet event cross-sections and ratio R_{32} .

The measured cross-sections after correcting for detector effects by using an iterative unfolding procedure are compared to the perturbative QCD predictions computed, using NLOJET++ program, at next-to-leading order (NLO) accuracy and complemented with non-perturbative (NP) corrections that are important at low $H_{T,2}/2$. The data are found to be well described by NLO calculations. The upwards trend observed in the inclusive 2-jet and 3-jet data at high $H_{T,2}/2$ in comparison to the prediction at NLO QCD, is explained by the onset of electroweak (EW) corrections in the 2-jet case. For the 3-jet event cross-sections these corrections have not yet been computed theoretically. In the 3-jet to 2-jet cross-section ratio R_{32} , the EW corrections are assumed to cancel. In fact, NLO QCD provides an adequate description of R_{32} in the accessible range of $H_{T,2}/2$. In contrast, leading order (LO) tree-level Monte Carlo (MC) predictions obtained using MADGRAPH5 event generator interfaced to PYTHIA6 exhibit significant deviations. The sources of experimental and theoretical uncertainties are studied in detail. The experimental uncertainty ranges from 4 to 32% for inclusive 2-jet event cross-sections, from 4 to 28% for 3-jet event cross-sections and from 1 to 28% for cross-section ratio R_{32} . It is dominated by the uncertainty due to the jet energy corrections (JEC) at lower $H_{T,2}/2$ values and by statistical uncertainty at higher $H_{T,2}/2$ values. The theoretical uncertainty ranges from 3 to 30% and 5 to 34% for inclusive 2-jet and 3-jet event cross-sections respectively and from 3 to 11% for ratio R_{32} . The PDF uncertainty derived with the CT10-NLO PDF set is the dominant source of theoretical uncertainty.

The inclusive multijet cross-sections being proportional to the powers of the strong coupling constant α_S ($\sigma_{n\text{-jet}} \propto \alpha_S^n$) are used to extract the value of the strong coupling constant at the scale of the Z boson mass $\alpha_s(M_Z)$. In cross-section ratio R_{32} which is proportional to α_S , many uncertainties and PDF dependencies largely cancel and hence becomes the better tool to extract the value of $\alpha_s(M_Z)$. In this thesis, a fit of the ratio of the inclusive 3-jet event cross-section to that of 2-jet, R_{32} in the range $300 < H_{T,2}/2 < 1680$ GeV, using the MSTW2008 PDF set gives :

$$\begin{aligned}\alpha_s(M_Z) &= 0.1150 \pm 0.0010 \text{ (exp)} \pm 0.0013 \text{ (PDF)} \pm 0.0015 \text{ (NP)} {}^{+0.0050}_{-0.0000} \text{ (scale)} \\ &= 0.1150 \pm 0.0023 \text{ (all except scale)} {}^{+0.0050}_{-0.0000} \text{ (scale)}\end{aligned}$$

and using the MMHT2014 PDF set gives :

$$\begin{aligned}\alpha_s(M_Z) &= 0.1142 \pm 0.0010 \text{ (exp)} \pm 0.0013 \text{ (PDF)} \pm 0.0014 \text{ (NP)} {}^{+0.0049}_{-0.0006} \text{ (scale)} \\ &= 0.1142 \pm 0.0022 \text{ (all except scale)} {}^{+0.0049}_{-0.0006} \text{ (scale)}\end{aligned}$$

The equally compatible values of $\alpha_s(M_Z)$ are determined with separate fits to the inclusive 2-jet and 3-jet event cross-sections provided the range in $H_{T,2}/2$ is restricted to $300 < H_{T,2}/2 < 1000$ GeV. The extracted $\alpha_s(M_Z)$ values in sub-ranges of $H_{T,2}/2$ are evolved to corresponding $\alpha_S(Q)$ along with the error bars at different scales Q . The current measurement of $\alpha_s(M_Z)$ and the running of $\alpha_S(Q)$ as a function of Q is in well agreement within uncertainties with the world average value of $\alpha_s(M_Z) = 0.1181 \pm 0.0011$ [21] and already existing determinations performed by the CMS and other experiments. The results on α_S reported here are consistent with the energy dependence predicted by the renormalization group equation (RGE) [18] which states that the strong force becomes weaker at short distances corresponding to large momentum transfers.

The inclusion of the EW corrections in inclusive 2-jet event cross-sections become relevant at $H_{T,2}/2$ beyond 1 TeV. Their availability for 3-jet one and hence cross-section ratio R_{32} can improve the precision of the measurement of $\alpha_s(M_Z)$. Also when the theoretical calculations will become available for inclusive 4-jet event

cross-sections, the various cross-section ratios such as $R_{43} \propto \alpha_S^1$ and $R_{42} \propto \alpha_S^2$ can be measured to extract the value of the strong coupling constant more precisely. Currently LHC is running at high center-of-mass energy of 13 TeV delivering a higher instantaneous luminosity and this makes possible to access the extended phase space and perform the measurements with improved accuracy.